Evaluation of the thermal neutron sensitivity, output linearity, and gamma-ray response of optical fiber-based neutron detectors using Li-glass scintillator

Akihisa Ishikawa[a, *], Kenichi Watanabe[b], Atsushi Yamazaki[a], Sachiko Yoshihashi[a], Shigefumi Imai[a], Akihiko Masuda[c], Tetsuro Matsumoto[c], Hiroki Tanaka[d], Yoshinori Sakurai[d], Mitsuhiro Nogami[e], Keitaro Hitomi[e], Akira Uritani[a], Hideki Harano[c]

[a]*Graduate School of Engineering, Nagoya University, Furo-cho, Chikusa-ku, Nagoya, Aichi 464-8603, Japan*

[b]*Graduate School of Engineering, Kyushu University, Motooka, Nishi-ku, Fukuoka 819-0395, Japan*

[c]*National Metrology Institute of Japan (NMIJ), National Institute of Advanced Industrial Science and Technology (AIST), 1-1-1 Umezono, Tsukuba, Ibaraki 305-8568, Japan*

[d]*Institute for Integrated Radiation and Nuclear Science, Kyoto University, 2 Asashiro-Nishi, Kumatori-cho, Sennan-gun, Osaka 590-0494, Japan*

[e]*Department of Quantum Science and Energy Engineering, Graduate School of Engineering, Tohoku University, 6-6-01 Aoba, Aramaki, Aoba-ku, Sendai, Miyagi 980-8579, Japan*

*** Corresponding author**

E-mail: ishikawa.akihisa@f.mbox.nagoya-u.ac.jp

Address: Graduate School of Engineering, Nagoya University, Furo-cho, Chikusa-ku, Nagoya, Aichi 464-8603, Japan

Telephone: +81-52-789-3846

FAX: +81-52-789-3844

Abstract

An optical fiber-based neutron detector can be used as a real-time neutron monitor for an intense neutron field. In this study, optical fiber-based neutron detectors were fabricated using Li-glass scintillator. The thermal neutron sensitivity, upper limit of the output linearity, and response to gamma rays from ^{60}Co and Cd were evaluated. The thermal neutron sensitivity was proportional to the mass of the Li-glass scintillator, and the calibration factor was 2.06×10^{-6} and 3.18×10^{-6} cps/(n/cm^2/s)/μg for the lower-level discrimination of the peak and valley channel of the neutron peak, respectively. The detector output linearity was confirmed to be up to nearly 2 Mcps. While evaluating the response to gamma rays, for both ^{60}Co and Cd, the gamma-ray counting rate was found to be smaller than the uncertainty associated with counting statistics in most expected applications where the neutron counting rate was >1 kcps.

Keywords: Neutrons, Gamma-rays, Optical Fiber-based Neutron Detectors, Real-time Measurements, Radiation Monitoring, Scintillator, Li-glass

1. Introduction

An optical fiber-based neutron detector can be a real-time neutron monitor for an intense neutron field [1,2]. Especially for boron neutron capture therapy (BNCT), the detector should count neutrons in the intense neutron flux up to 10^9 neutrons/cm^2/s and should not distort the target neutron field. Therefore, the relatively low neutron sensitivity and small size of the optical fiber-based detector is an advantage. In our group, some types of optical fiber-based neutron detectors and experimental methods using these detectors for characterization of the intense neutron field for BNCT have been developed [1,3-5]. To measure the intense neutron field, the detector is required to have proper thermal neutron sensitivity, a wide dynamic range, and a low sensitivity to the gamma rays coexisting in the neutron field. Our detector shows a peak structure, corresponding to neutron events in the signal pulse height spectrum, the so-called neutron peak. Conversely, for the gamma-ray events, pulse heights are suppressed and show an exponentially decreasing distribution in the low pulse-height region. This condition occurs because our detectors use a small-sized neutron scintillator, in which the energetically-charged particles generated in ^{6}Li(n,t) reactions can deposit the entire energy; however, fast electrons generated in gamma-ray interactions escape from the scintillator before depositing their energy [1]. In a previous study, we used the Li-glass scintillator in the detector and evaluated the pulse height spectrum, radiation hardness, and output linearity [6]. The Li-glass scintillator-based detectors are well-known to show an excellent counting rate capability [7,8]. Also, several experimental results of characterization, such as the counting characteristic, intrinsic efficiency for incident neutron and neutron-gamma discrimination, of some different types of neutron detectors using the Li-glass scintillator have been reported [9-14]. However, for this type of detector using the small piece of the Li-glass scintillator with the 10-meters-long optical fiber to be usable as a counting-mode detector in the intense neutron fields, the neutron sensitivity, maximum counting rate, and gamma-ray sensitivity have never been evaluated. The detectors used in medical practice are strongly desired to confer to the traceability of the national standard. In many nations, the thermal neutron standard field is a graphite pile with (α,n) reaction-based neutron source like Pu-Be or Am-Be sources. The neutron flux in this type of standard field is not that high; therefore, it is difficult to calibrate the low sensitivity detectors. In order to cover both fields, i.e., the standard and BNCT, the detector should have a wide dynamic range. The Li-glass scintillator-based detector might be suitable because of its excellent counting rate capability. Therefore, this study aimed to evaluate the thermal neutron sensitivity at the national standard neutron facility in the National Institute of Advanced

Industrial Science and Technology (AIST), Japan. Additionally, the upper limit of the detector output linearity and its response to gamma rays were also evaluated.

2. Materials and Methods

2.1. Optical fiber-based neutron detector using a Li-glass scintillator

Figure 1 shows the cross-sectional structure of the optical fiber-based neutron detector. The incident neutrons react with ^{6}Li atoms in the Li-glass scintillator (GS20, Scintacor, Cambridge, England), and α-particles and tritons generated in ^{6}Li(n,t)α reactions deposit their energy in the scintillator and induce scintillation. The emitted scintillation photons are transmitted to the quartz optical fiber (FP600URT, Thorlabs, New Jersey, United States) and converted into photoelectrons in the photomultiplier tube (PMT, R9880U-210, Hamamatsu Photonics, Shizuoka, Japan). The core diameter and numerical aperture of the optical fiber are 600 μm and 0.5, respectively. The attenuation of the quartz optical fiber is ~70 dB/km at the maximum emission wavelength of the Li-glass scintillator; thus, the transmission loss is estimated to be ~15% for a length of 10 m. The small piece of the Li-glass scintillator is attached to the tip of the optical fiber using the ultraviolet (UV)-curable resin (NOA63, Norland, New Jersey, United States) with ~100% of the transmittance at the emission wavelength of the Li-glass scintillator. The mass of the small piece of the Li-glass scintillator is measured in advance using a precise electronic balance (BM20, A&D Comp., Tokyo, Japan). To efficiently collect the scintillation photons, the scintillator attached to the tip of the optical fiber is covered with the diffusive reflective coating of TiO_2 powder (Titanium (IV) Oxide, Wako Pure Chemical, Osaka, Japan). The outermost layer is shaded and protected by the heat shrinkage tube (SETC-2.0B-10, Denka Electron, Tokyo, Japan). The tip of the optical fiber-based neutron detector, which cannot be completely shaded only by the heat shrinkage tube, is shaded by a carbon rod with a diameter of

1 mm and length of 10 mm as a shading material that is hardly activated by neutron irradiation.

The properties of the optical fiber-based neutron detectors fabricated for this study are listed in Table 1. The small pieces of the scintillators with mass ranging from 18 to 141 μg were used to fabricate six optical fiber-based neutron detectors. Two of them were fabricated using several small pieces to check the suppressing effect on the gamma-ray sensitivity. The gamma-ray sensitivity is expected to decrease with decreasing scintillator size because the fast electrons generated in gamma-ray interactions can easily escape. Contrarily, the neutron sensitivity depends on the total amount of ^{6}Li.

Table 1. The properties of the fabricated detectors.

Detector ID	Li-glass scintillator		Sensitivity	Linearity	γ-ray test	
	Quantity [−]	Mass [μg]	evaluation	test	^{60}Co	Cd
No. 0	None	0			✓	
No. 1	Single	18 ± 1			✓	
No. 2	Plural (3 pieces)	32 ± 2	✓		✓	✓
No. 3	Single	47 ± 2			✓	
No. 4	Plural (4 pieces)	103 ± 2	✓		✓	✓
No. 5	Single	108 ± 4			✓	
No. 6	Single	141 ± 2	✓	✓	✓	✓

2.2. Signal processing

Figure 2 shows the signal processing circuits of the optical fiber-based neutron detector system. The anode signal of the PMT is directly fed into the digital multichannel analyzer (digital MCA, HSMCA 4414-L-NW, ANSeeN, Shizuoka, Japan), with high-voltage supply and signal integration function. In this digital MCA, the PMT signal is integrated with a proper time constant, digitized with the analog–digital converter, and then processed in the field-programmable gate array. The digital MCA has four input channels to process simultaneously and records the list-mode event data of the pulse height, rise time, and time stamp of events.

To determine the setup of the digital MCA, thermal neutron response evaluation experiments have been conducted. The evaluation experiments were performed at the thermal neutron port E3, with a neutron guide tube with curvature to derive thermal neutrons from the reactor in the Kyoto University Research Reactor (KUR) at the Institute for Integrated Radiation and Nuclear Science of Kyoto University, Japan. In this neutron port, gamma rays from the reactor are well suppressed because the reactor core is not directly visible in this port. The measurement parameters of the digital MCA, such as the applied voltage to the PMT and the time constant of the integrating circuit, were determined to create a clear neutron peak in the pulse height spectrum. Figure 3 shows an example of the signal pulse height spectrum. The lower-level discrimination (LLD) was determined for two settings: the first and second settings, with LLDs set at the valley and peak channels in the pulse height spectrum, respectively.

2.3. Thermal neutron sensitivity evaluation

The thermal neutron sensitivity was evaluated for detector Nos. 2, 4, and 6 listed in Table 1. The sensitivity evaluation was performed at the neutron standard field in the AIST, Japan [15]. The neutron standard field is created in the graphite pile with an ^{241}Am-Be neutron source. Optical fiber-based neutron detectors were placed at the reference point inside the graphite pile at a distance of 900 mm from the Am-Be source, as shown in Figure 4. The pulse height spectra were obtained for neutron irradiation and background condition.

2.4. Output linearity evaluation

The detector output linearity was evaluated using an accelerator-based neutron source in the Aomori prefecture Quantum Science Center, Japan. Neutrons are produced by 20 MeV protons bombarding a Be target. The neutron radiography beam port was used in this experiment. The proton beam current could be tuned from 10 to 50 μA to change the neutron intensity. Detector No. 6 (141 μg) in Table 6 was used to evaluate the upper limit of the counting rate on the output linearity. As a reference detector to monitor the neutron intensity fluctuation, neutrons were simultaneously measured using detector No. 2 listed in Table 1, which has a lower sensitivity than detector No. 6 and is expected to keep the output linearity to higher neutron intensity. When the proton current was 10 μA, the thermal neutron flux at the detector position was derived using the thermal neutron sensitivity calibrated at the neutron standard field in the AIST as discussed in 2.3. For the higher proton current conditions, the neutron flux was assumed to be proportional to the proton current. This proportionality was also examined using detector No. 2 listed in Table 1 as a reference detector with low sensitivity.

2.5. Response evaluation for prompt gamma rays from Cd

Cadmium (Cd) is one of the elements used as a neutron-shielding material. ^{113}Cd has the largest neutron capture cross section for thermal neutrons among the Cd isotopes with isotopic abundance of 12.2%. Moreover, ^{113}Cd has a unique shape of neutron absorption cross section and can absorb thermal neutrons only. Therefore, this material is used to evaluate the thermal neutron response using the Cd subtraction method. After absorbing the neutrons, Cd isotopes emit prompt gamma rays. In this section, we evaluate the detector response to the prompt gamma rays from Cd.

The detector response to Cd gamma rays was acquired at the thermal neutron port E3 in the

KUR. The experimental setup is shown in Figure 5. The detector head was covered with a Cd tube with a 0.5 mm thickness and 44 mm length; therefore, thermal neutrons were completely cut and the detector was only exposed to prompt gamma rays from Cd. The pulse height spectra were measured, and the counting rate of gamma-ray events was evaluated for two LLD conditions, set at the valley and peak channels in the pulse height spectrum. The measurements were performed for detector Nos. 2, 4, and 6 listed in Table 1.

2.6. Response evaluation for intense gamma ray from ^{60}Co

In general, MeV-order gamma rays exist in a majority of neutron experiments due to nuclear reactions between neutrons and various materials, such as $^{1}H(n,\gamma)^{2}H$ reactions, causing false counting rates in neutron detectors.

Measurements to evaluate the detector response to ^{60}Co gamma rays were performed at the ^{60}Co gamma-ray irradiation facility of Nagoya University, Japan. The gamma-ray dose rate at the detector position was measured using an ionization chamber (PTW Freiburg, TN30013). The optical fiber-based neutron detectors and ionization chamber were fixed between two polyethylene blocks ($50 \times 100 \times 200$ mm^3) as shown in Figure 6. The measurement points were at a distance of 700, 1000, and 1400 mm from the center of the ^{60}Co source, and the gamma-ray dose rate measured by the ionization chamber were 7.50, 3.68, and 1.90 Gy/h, respectively. The pulse height spectra were measured, and the counting rate of the gamma-ray events was evaluated for two LLD conditions set at the valley and peak channels. These measurements were performed for all detectors in Table 1. Furthermore, to evaluate the scintillation of the optical fiber itself using the gamma ray from the ^{60}Co source, a dummy detector without the Li-glass scintillator, detector No. 0 listed in Table 1, was also fabricated, and the gamma-ray counting rate was evaluated. Measurements with the dummy detector were performed with the same PMT and MCA parameters as detector No. 6 listed in Table 1.

3. Results and Discussions

3.1. Thermal neutron sensitivity

Figure 7 shows the thermal neutron sensitivity as a function of the mass of the Li-glass scintillators for detector Nos. 2, 4, and 6 listed in Table 1. Although the deviation due to the gamma-ray counts discussed in Section 3.3 is partially observed when the LLD is set at the valley channel, the thermal neutron sensitivity is approximately proportional to the scintillator mass. Therefore, the calibration factor was obtained as 2.06×10^{-6} and 3.18×10^{-6} cps/(n/cm^2/s)/μg for the LLD settings set at the peak and valley channels of the neutron peak, respectively.

3.2. Output linearity

Figure 8 shows the detector counting rate as a function of thermal neutron flux. The output linearity is confirmed up to ~2 Mcps and is broken down because of distorted pulse height spectrum due to the pulse pile-up effect above 2 Mcps. Compared with the optical fiber-based neutron detector using the LiF/Eu:CaF_2 scintillator used in a previous study [4], the detector used in this study shows excellent output linearity even under nearly 40 times larger counting rate due to the fast decay time constant of the Li-glass. For real-time measurements, the detector counting rate of about 1 kcps is needed at the minimum. Since the upper limit of the detector counting rate is 2Mcps, a dynamic range of 3 digits or more is achieved in our detector.

3.3. Response to prompt gamma ray from Cd

Figure 9 shows the pulse height spectra of detector No. 2 listed in Table 1 when irradiated with thermal neutrons and prompt gamma rays from Cd. The background spectrum has also been plotted. Figure 10 shows the counting rate ratio of the gamma-ray events (C_γ) to that of the neutron events (C_n) [cps/kcps] as a function of the mass of the Li-glass scintillator. The C_γ/C_n ratio for each LLD conditions of the valley and peak channels in the neutron peak is evaluated to be 0.01% and 0.25%, respectively, for detector No. 6 listed in Table 1, which is the maximum mass in this experiment and is the worst case from the viewpoint of the gamma-ray suppression ability.

3.4. Response to the intense gamma ray from the ^{60}Co source

Figure 11 shows the pulse height spectra of detector No. 2 listed in Table 1 with the Li-glass scintillator with a mass of 32 μg when irradiated with intense gamma rays from the ^{60}Co source at gamma-ray dose rate of 1.90, 3.68, and 7.50 Gy/h. The spectrum obtained when irradiating with thermal neutrons has also been plotted.

Figure 12 shows the gamma counting rate as a function of dose rate for detector Nos. 6 and 2 listed in Table 1 with the Li-glass scintillator with mass of 141 and 32 μg, respectively, in which the highest and lowest gamma-ray sensitivities of all detectors in this study are expected. When the LLD was set at the neutron peak channel, the counting rate of the gamma-ray events was <3 cps under 7.5 Gy/h, even in the detector with the highest gamma-ray sensitivity. When the LLD is set at the valley channel, the gamma-ray counting rate reaches 190 cps at gamma-ray dose rate of 7.50 Gy/h in the same detector. However, the detector using the plural small pieces of the Li-glass scintillator with total mass of 32 μg expectedly showed the lowest gamma-ray sensitivity among all detectors in this study; therefore, the counting rate of gamma-ray events is not available when the LLD is set at the peak channel and is smaller than the uncertainty associated with counting statistics even when the LLD is set at the valley channel.

Figure 13 shows the dependency of the counting rate in gamma-ray events at a gamma-ray dose rate of 7.50 Gy/h on the mass of the Li-glass scintillator when the LLD is set at both, the peak and valley channels. Results of the dummy detector without the Li-glass scintillator are plotted with a mass of 0 μg. The counting rate of gamma-ray events roughly depends on the Li-glass scintillator mass. However, the gamma-ray sensitivity is not significantly changed between detectors using single and plural scintillators, indicating that the gamma-ray sensitivity is not effectively suppressed using several small pieces of the Li-glass scintillator instead of the single small piece. This is considered to be due to the escaped fast electrons, which might reenter to an adjacent scintillator and deposit their energy.

The counting rate of gamma-ray events is >100 cps for three detectors using Li-glass scintillators with a mass of >100 μg when the LLD is set at the valley channel. Furthermore, results indicated that the optical fiber scintillation itself is considered to be negligible.

Since fast electrons induced by high energy gamma-rays have low stopping power, the signal pulse heights by higher energy gamma-rays more than 1 MeV are lower in the small size scintillator [1]. In this study, we evaluated the counting rates for 1.17 and 1.33 MeV gamma-rays from the ^{60}Co source, however, those by higher energy gamma-rays are considered to be similar level.

4. Conclusions

In this paper, various specifications of the optical fiber-based neutron detector, such as the thermal neutron sensitivity, detector output linearity, and gamma-ray sensitivity, are experimentally confirmed using the Li-glass scintillator. The thermal neutron sensitivity per unit scintillator mass is calibrated to be 2.06×10^{-6} and 3.18×10^{-6} cps/(n/cm^2/s)/μg when the LLD is set at the peak and valley channels in the pulse height spectra, respectively. The upper limit of the detector output linearity of the fabricated optical fiber-based neutron detector is evaluated. Therefore, the detector output linearity is confirmed up to ~2 Mcps, which is ~40 times larger than the upper limit of the conventional detectors using LiF/Eu:CaF_2 scintillators. The gamma-ray response is also evaluated. For gamma rays from the ^{60}Co source, the counting rate of the gamma-ray events is >100 cps at the gamma-ray dose rate of 7.50 Gy/h for detectors using the Li-glass scintillator with a mass of >100 μg when the LLD is set at the valley channel. On the other hand, the counting rate when the LLD is set at the peak channel is <3 cps for the same detectors even at the gamma-ray dose rate of 7.50 Gy/h. Furthermore, for lower gamma-ray dose rates, the counting rates are negligibly small. The sensitivity to prompt gamma rays from Cd is much smaller than thermal neutrons. The ratio of the counting rate of the prompt gamma-ray events from Cd to that of the thermal neutron events is approximately 0.25% even when the LLD is set at the valley channel. In conclusion, the gamma-ray counting rate will be smaller than the uncertainty associated with counting statistics in most expected applications where the neutron counting rate is estimated to be >1 kcps. These results indicates that our detector can offer a high-precision real-time neutron measurements with the traceable neutron sensitivity, wide dynamic range, and high neutron-gamma discrimination in the intense neutron fields, and is helpful in neutron monitoring and quality assurance works in BNCT applications.

Acknowledgments

Funding: This work was partially supported by JSPS KAKENHI Grant Number JP20J21215 and the Precise Measurement Technology Promotion Foundation.

The authors would like to thank Enago (www.enago.jp) for the English language review.

References

[1] K. Watanabe, Y. Kawabata, A. Yamazaki, A. Uritani, T. Iguchi, K. Fukuda, T. Yanagida, Development of an optical fiber type detector using a $EuLiCaAlF_6$ scintillator for neutron monitoring in boron neutron capture therapy, Nuclear Instruments and Methods in Physics Research Section A, 802 (2015) 1-4. https://doi.org/10.1016/j.nima.2015.08.056

[2] M. Takada, T. Nunomiya, A. Masuda, T. Matsumoto, H. Tanaka, S. Nakamura, S. Endo, M. Nakamura, K. Aoyama, O. Ueda, M. Narita, T. Nakamura, Development of a real-time neutron beam detector for boron neutron capture therapy using a thin silicon sensor, Applied Radiation and Isotopes, 176 (2021) 109856. https://doi.org/10.1016/j.apradiso.2021.109856

[3] A. Ishikawa, A. Yamazaki, K. Watanabe, S. Yoshihashi, A. Uritani, K. Fukuda, A. Koike, R. Ogawara, M. Suda, T. Hamano, Sensitivity and linearity of optical fiber-based neutron detectors using small ^{6}Li-based scintillators, Nuclear Instruments and Methods in Physics Research Section A, 954 (2020) 161661. https://doi.org/10.1016/j.nima.2018.11.120

[4] A. Ishikawa, A. Yamazaki, K. Watanabe, S. Yoshihashi, A. Uritani, Y. Tsurita, K. Tsuchida, Y. Kiyanagi, A comparison between simulation and experimental results for depth profile of ^{6}Li reaction rate in a water phantom of BNCT using a small ^{6}Li-based scintillator neutron detector with an optical fiber, Radiation Measurements, 133, 106270 (2020). https://doi.org/10.1016/j.radmeas.2020.106270

[5] K. Watanabe, S. Yoshihashi, A. Ishikawa, S. Honda, A. Yamazaki, Y. Tsurita, A. Uritani, K. Tsuchida, Y. Kiyanagi, First experimental verification of the neutron field of Nagoya University Accelerator-driven neutron source for boron neutron capture therapy, Applied Radiation and Isotopes, 168, 109553 (2021). https://doi.org/10.1016/j.apradiso.2020.109553

[6] A. Ishikawa, K. Watanabe, A. Yamazaki, S. Yoshihashi, A. Uritani, Development of optical-fiber-based neutron detector using Li glass scintillator for an intense neutron field, Sensors and

Materials, 32 (2020) 1489-1495. https://doi.org/10.18494/SAM.2020.2748

[7] K. Toh, M. Katagiri, K. Sakasai, M. Matsubayashi, A. Birumachi, H. Takahashi, M. Nakazawa, High counting rate two-dimensional neutron-imaging method using rectangular scintillators with WLS fibers, Applied Physics A 74, s1601-s1603 (2002). https://doi.org/10.1007/s003390201834

[8] S. Endo, H. M. Shimizu, M, Kitaguchi, K. Hirota, S. Satoh, T. Kai, T. Okudaira, C. C. Haddock, N. Oi, F. Goto, I. Ito, M. Nakaji, S. Takada, J. Koga, T. Yoshioka, K. Sakai, Development of high-counting-rate neutron detector for CP-violation search in neutron-induced reactions, JPS Conf. Proc. 22, 011021 (2018). https://doi.org/10.7566/JPSCP.22.011021

[9] K. Mizukami, S. Sato, H. Sagehashi, S. Ohnuma, M. Ooi, H. Iwasa, F. Hiraga, T. Kamiyama, Y. Kiyanagi, Measurements of performance of a pixel-type two-dimensional position sensitive Li-glass neutron detector, Nuclear Instruments and Methods in Physics Research Section A, Volume 529, Issue 1-3, 310-312 (2004). https://doi.org/10.1016/j.nima.2004.05.001

[10] T. Matsumoto, H. Harano, T. Shimoyama, A. Uritani, Y. Sakurai and K. Kudo, Development of a novel small-sized neutron detector based on a /sup 6/Li-glass scintillator, IEEE Nuclear Science Symposium Conference Record, 2005, 1291-1293 (2005). https://doi.org/10.1109/NSSMIC.2005.1596556

[11] K.D. Ianakiev, M.P. Hehlen, M.T. Swinhoe, A. Favalli, M.L. Iliev, T.C. Lin, B.L. Bennett, M.T. Barker, Neutron detector based on Particles of 6Li glass scintillator dispersed in organic lightguide matrix, Nuclear Instruments and Methods in Physics Research Section A, 784, 189-193 (2015). https://doi.org/10.1016/j.nima.2014.10.073

[12] M. Mayer, J. Nattress, V. Kukharev, A. Foster, A. Meddeb, C. Trivelpiece, Z. Ounaies, I. Jovanovic, Development and characterization of a neutron detector based on a lithium glass-

polymer composite, Nuclear Instruments and Methods in Physics Research Section A, 785, 117-122 (2015). https://doi.org/10.1016/j.nima.2015.03.014

[13] G.C. Rich, K. Kazkaz, H.P. Martinez, T. Gushue, Fabrication and characterization of a lithium-glass-based composite neutron detector, Nuclear Instruments and Methods in Physics Research Section A, 794, 15-24 (2015). https://doi.org/10.1016/j.nima.2015.05.004

[14] C. L. Wang, R. A. Riedel, Improved neutron-gamma discrimination for a ^{6}Li-glass neutron detector using digital signal analysis methods, Rev. Sci. Instrum. 87, 013301 (2016). https://doi.org/10.1063/1.4939821

[15] R. Nolte, R. Boettger, J. Chen, H. Harano, D. J. Thomas, International key comparison of thermal neutron fluence measurements─CCRI(III)-K8, Metrologia, 52 (2015) 06011. http://doi.org/10.1088/0026-1394/52/1A/06011

Figure Captions

Figure 1. The cross-sectional structure of the optical fiber-based neutron detector.

Figure 2. The signal processing circuits of the optical fiber-based neutron detector system. SMA, sub miniature A. PMT, photomultiplier tube. SHV, safe high voltage. BNC, Bayonet Neill-Concelman. DC, direct current. PC, personal computer. MCA, multichannel analyzer.

Figure 3 An example of the pulse height spectrum obtained from the optical fiber-based detector. There are two patterns of the LLD settings: the valley and peak channel in the pulse height spectrum. LLD, lower-level discrimination.

Figure 4. The experimental setup at the graphite pile neutron standard in the National Institute of Advanced Industrial Science and Technology.

Figure 5. The experimental setup for irradiation with a) thermal neutrons and b) prompt gamma rays from Cd at the port E3 in the Kyoto University Research Reactor.

Figure 6. The experimental setup at the ^{60}Co gamma-ray irradiation facility of Nagoya University.

Figure 7. The relationship between thermal neutron sensitivity and the mass of the Li-glass scintillator of detector Nos. 2, 4, and 6 listed in Table 1 for the lower-level discrimination (LLD) setting set at the a) peak and b) valley channels in the pulse height spectrum.

Figure 8. The detector counting rate as a function of thermal neutron flux for the proton beam current from 10 to 50 μA.

Figure 9. The pulse height spectra of detector No. 2 listed in Table 1, when irradiating with thermal neutrons and prompt gamma rays from the cadmium tube. The background spectrum has also been plotted. The neutron counting rate is plotted to the left (Y) axis. The gamma-ray and background counting rates are plotted to the right (R) axis.

Figure 10. The ratio of the counting rate in the gamma-ray events (C_γ) as compared to that of the neutron events (C_n) [cps/kcps] as a function of mass of the Li-glass scintillator [μg].

Figure 11. The pulse height spectra of detector No. 2 listed in Table 1 when irradiated with gamma rays from the ^{60}Co source at the gamma-ray dose rate of 1.90, 3.68, and 7.50 Gy/h. The spectrum when irradiated with thermal neutrons has also been plotted.

Figure 12. The gamma-ray dose rate dependency of the counting rate in gamma-ray events for the detector using the Li-glass scintillator with mass of 141 and 32 μg. LLD, lower-level discrimination.

Figure 13. The dependency of the counting rate in gamma-ray events at the gamma-ray dose rate of 7.50 Gy/h on the mass of the Li-glass scintillator when the lower-level discrimination (LLD) is set at the a) peak and b) valley channels in the neutron peak.

Figure 1

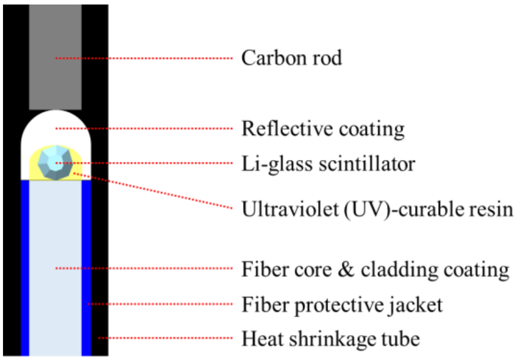

Carbon rod
Reflective coating
Li-glass scintillator
Ultraviolet (UV)-curable resin
Fiber core & cladding coating
Fiber protective jacket
Heat shrinkage tube

Figure 2

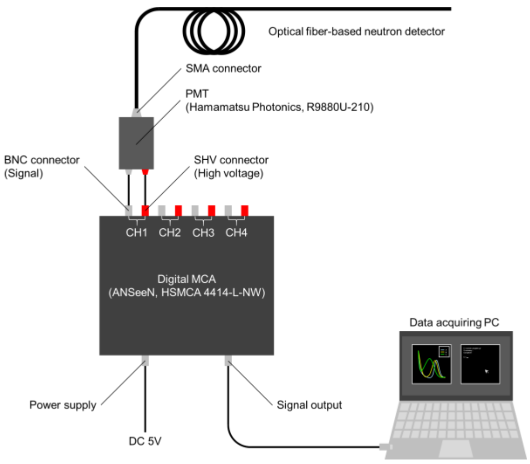

Optical fiber-based neutron detector
SMA connector
PMT
(Hamamatsu Photonics, R9880U-210)
BNC connector
(Signal)
SHV connector
(High voltage)
CH1
CH2
CH3
CH4
Digital MCA
(ANSeeN, HSMCA 4414-L-NW)
Data acquiring PC
Power supply
Signal output
DC 5V

Figure 3

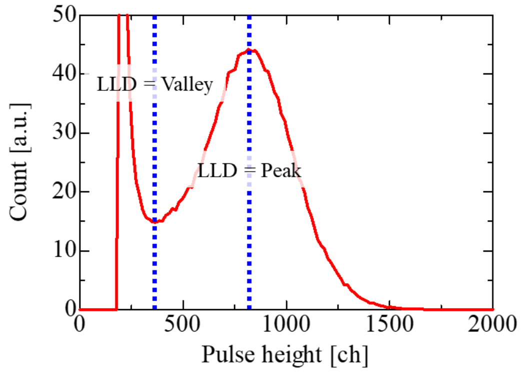

LLD = Valley
LLD = Peak
Count [a.u.]
50
40
30
20
10
0
0
500
1000
1500
2000
Pulse height [ch]

Figure 4

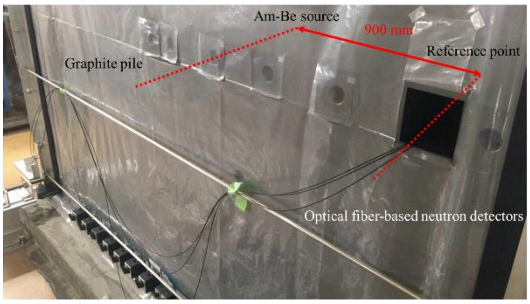
Am-Be source
900 mm
Reference point
Graphite pile
Optical fiber-based neutron detectors

Figure 5

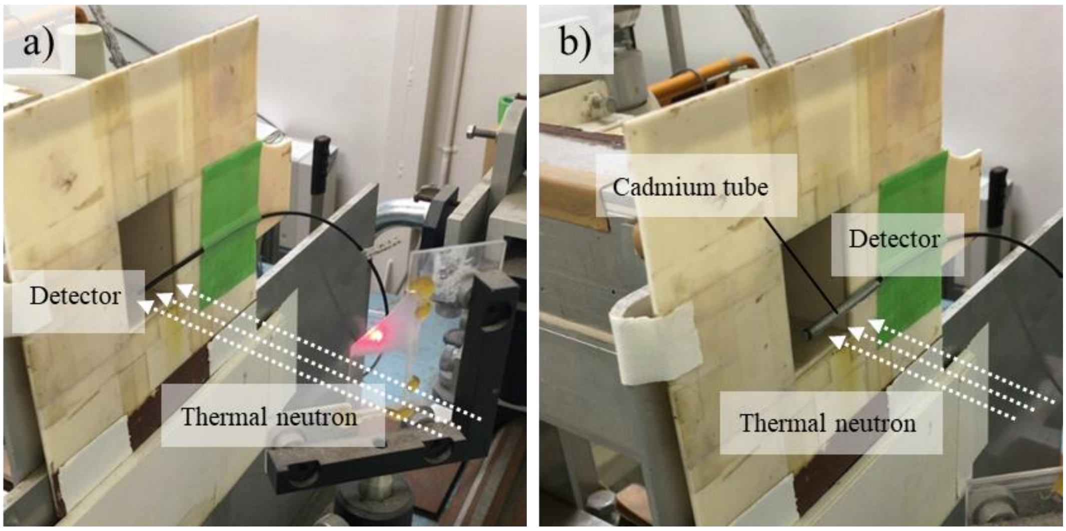

a)
Detector
Thermal neutron
b)
Cadmium tube
Detector
Thermal neutron

Figure 6

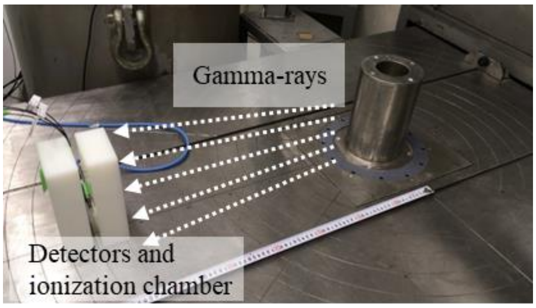

Figure 7

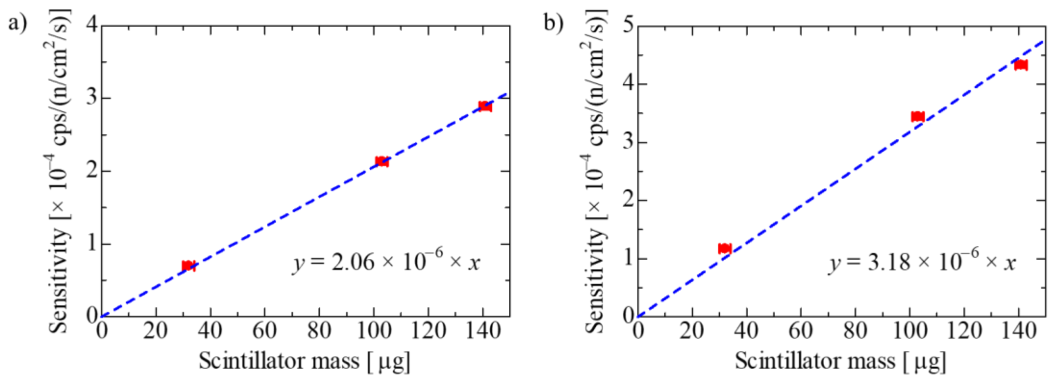

a)
Sensitivity [× 10^{-4} cps/(n/cm^2/s)]
Scintillator mass [μg]
$y = 2.06 \times 10^{-6} \times x$
0
1
2
3
4
0
20
40
60
80
100
120
140
b)
Sensitivity [× 10^{-4} cps/(n/cm^2/s)]
Scintillator mass [μg]
$y = 3.18 \times 10^{-6} \times x$
0
1
2
3
4
5
0
20
40
60
80
100
120
140

Figure 8

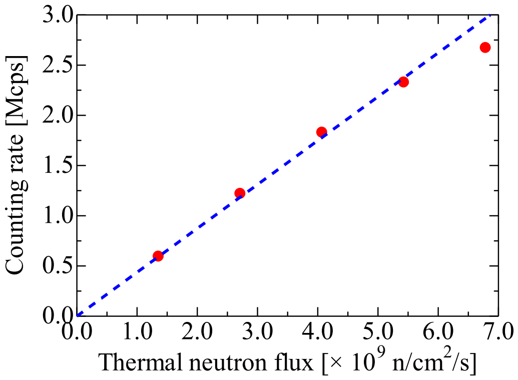

3.0
2.5
2.0
1.5
1.0
0.5
0.0
Counting rate [Mcps]
0.0
1.0
2.0
3.0
4.0
5.0
6.0
7.0
Thermal neutron flux [× 10^9 n/cm^2/s]

Figure 9

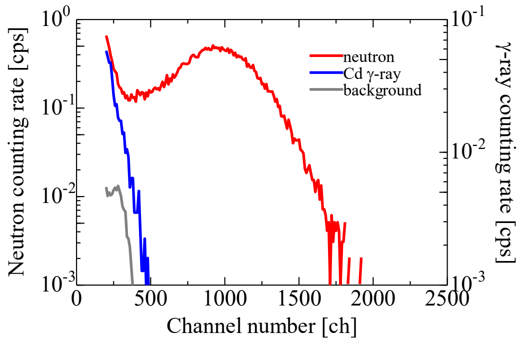

neutron
Cd γ-ray
background
Neutron counting rate [cps]
γ-ray counting rate [cps]
Channel number [ch]
10^0
10^-1
10^-2
10^-3
0
500
1000
1500
2000
2500

Figure 10

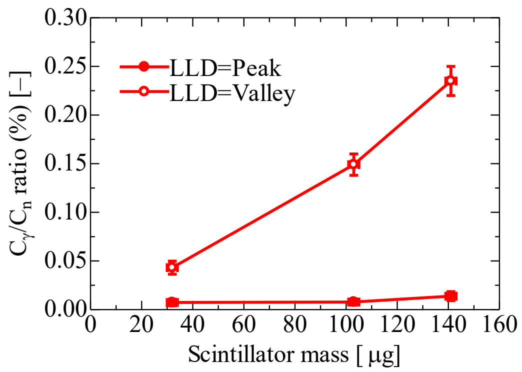

0.30
0.25
0.20
0.15
0.10
0.05
0.00
LLD=Peak
LLD=Valley
C_γ/C_n ratio (%) [–]
0
20
40
60
80
100
120
140
160
Scintillator mass [μg]

Figure 11

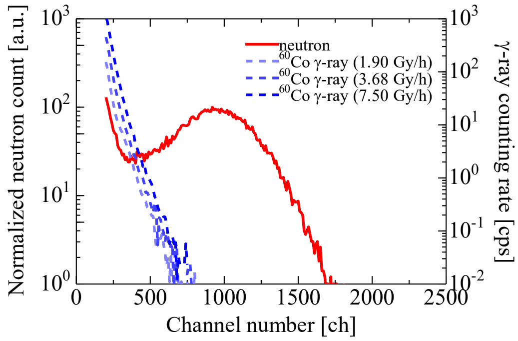

Normalized neutron count [a.u.]
γ-ray counting rate [cps]
Channel number [ch]
neutron
60Co γ-ray (1.90 Gy/h)
60Co γ-ray (3.68 Gy/h)
60Co γ-ray (7.50 Gy/h)
10^3
10^2
10^1
10^0
10^-1
10^-2
0
500
1000
1500
2000
2500

Figure 12

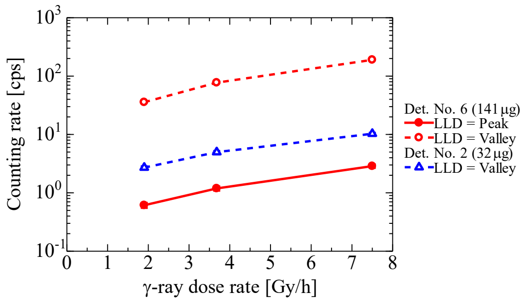

Counting rate [cps]
10^3
10^2
10^1
10^0
10^-1
0
1
2
3
4
5
6
7
8
γ-ray dose rate [Gy/h]
Det. No. 6 (141 μg)
LLD = Peak
LLD = Valley
Det. No. 2 (32 μg)
LLD = Valley

Figure 13

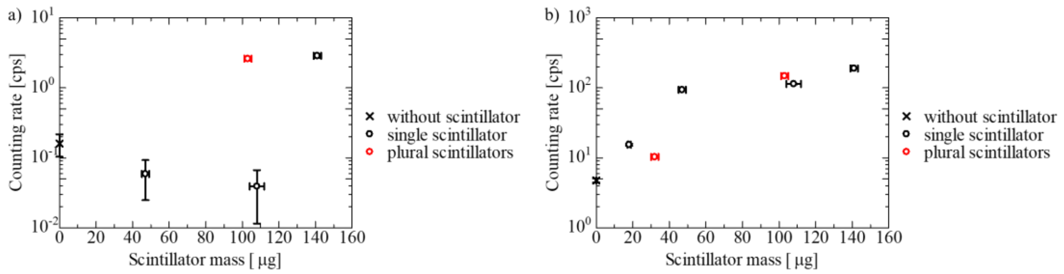

a)
b)
Counting rate [cps]
Scintillator mass [μg]
without scintillator
single scintillator
plural scintillators